Recibido: 19/02/2026
Aceptado: 11/05/2026
Disponible en línea: 25/05/2026
Publicado: 31/07/2026

**REVISTA DE TELEDETECCIÓN**
Asociación Española de Teledetección
(2026) 68, e25679
EISSN 1988-8740
https://doi.org/10.4995/raet.2026.25679

# Transfer learning in convolutional neural networks for fire scene classification in the Pantanal Biome (Brazil)

Jack Endrick Pastrana-Mojica [1*], Tássia Fraga-Belloli [1], Pamela Boelter-Herrmann [1], Ana Júlia Magalhães-Gonçalves Dias [2], Deyvis Cano [1], Camila Souza-Silva [3], Daniel Capella-Zanotta [4]

[1] *Programa de Pós-Graduação em Sensoriamento Remoto, Universidade Federal do Rio Grande do Sul, Brazil.*
[2] *Programa de Pós-Graduação em Sensoriamento Remoto, Instituto Nacional de Pesquisas Espaciais, Brazil.*
[3] *Instituto Brasileiro do Meio Ambiente e dos Recursos Naturais Renováveis, Brazil.*
[4] *Universidade do Vale do Rio dos Sinos, Brazil.*

Resultados destacados:

- Transfer learning improved image scene classification accuracy.
- EuroSAT images improved intra-domain transfer learning performance
- The VGG-19 architecture achieved accuracy above 95%.
- The SWIR band was the most important feature for burned area classification.

**Abstract:** During 2024, wildfires in the Pantanal, Brazil, posed a significant threat to the world's largest wetland. This study presents a scene classification approach using Sentinel-2 imagery from fire-affected and non-affected areas, based on deep learning techniques. First, a model was experimentally trained using the EuroSAT dataset to classify grasslands and herbaceous vegetation. Subsequently, a transfer learning technique was applied to images of the fire-affected Pantanal. Finally, the Visual Geometry Group (VGG-19) architecture was trained from scratch, without using pretrained parameters. Considering these three experiments, training with the EuroSAT dataset achieved a loss of 0.202 after 50 epochs. The model with transfer learning, using the weights learned during the experimental training, obtained a validation loss of 0.15 and an accuracy of 95%, whereas training from scratch reached a validation loss of 0.07 and an accuracy of 97%. The results indicate similar performance between the two strategies, demonstrating that in-domain training can be considered an effective method for training CNNs applied to satellite imagery, without compromising classification accuracy, even in the presence of significant differences in the contextual information of the images. This approach is presented as a methodological alternative for environmental monitoring in complex tropical regions, characterized by high spatial and spectral heterogeneity.

**Keywords:** convolutional neural networks (CNNs), tropical ecosystems, transfer learning, Pantanal, forest fires.

## Aprendizaje por transferencia en redes neuronales convolucionales para la clasificación de escenas de incendios en el bioma Pantanal (Brasil)

**Resumen:** Durante 2024, los incendios en el Pantanal, Brasil, representaron una amenaza significativa para el humedal más grande del mundo. Este estudio presenta un enfoque de clasificación de escenas utilizando imágenes Sentinel-2 de áreas afectadas y no afectadas por el fuego, basado en aprendizaje profundo. En primer

**To cite this article:** Pastrana-Mojica, J.E., Fraga-Belloli, T., Boelter-Herrmann, P., Magalhães-Gonçalves Dias, A.J., Cano, D., Souza-Silva, C., Capella-Zanotta, D. 2026. Transfer learning in convolutional neural networks for fire scene classification in the Pantanal Biome (Brazil). *Revista de Teledetección*, *68*, e25679. https://doi.org/10.4995/raet.2026.25679

* *Corresponding author: jack.pastrana@ufrgs.br*

lugar, se entrenó experimentalmente un modelo con el conjunto de datos EuroSAT para clasificar pastizales y vegetación herbácea. Posteriormente, se aplicó la técnica de transferencia de aprendizaje a las imágenes del Pantanal afectadas por incendios. Finalmente, la arquitectura Grupo de Geometría Visual (VGG-19) fue entrenada desde cero, sin el uso de parámetros preentrenados. Considerando estos tres experimentos, el entrenamiento con el conjunto EuroSAT alcanzó una pérdida de 0.202 tras 50 épocas. El modelo con transferencia de aprendizaje, utilizando los pesos aprendidos en el entrenamiento experimental, obtuvo una pérdida de validación de 0.15 y una precisión del 95 %, mientras que el entrenamiento desde cero alcanzó una pérdida de validación de 0.07 y una precisión del 97 %. Los resultados indican un desempeño similar entre las dos estrategias, lo que evidencia que el entrenamiento intradominio puede considerarse un método eficaz para el entrenamiento de CNNS aplicadas a imágenes satelitales, sin comprometer la precisión en la clasificación de escenas, incluso en presencia de diferencias significativas en las informaciones contextuales de las imágenes. Este enfoque se presenta como una alternativa metodológica para el monitoreo ambiental en regiones tropicales complejas, caracterizadas por una alta heterogeneidad espacial y espectral.

**Palabras clave:** redes neuronales convolucionales (CNNs), ecosistemas tropicales, transferencia de aprendizaje, Pantanal, incendios forestales.

## 1. Introducción

The Pantanal, the largest tropical wetland in the world, covers an area of approximately 138,183 km², located roughly between latitudes 16° S and 22° S and longitudes 55° W and 58° W, encompassing areas of Brazil, Bolivia, and Paraguay (IBGE, 2022). It is characterized by a seasonal flood and drought regime, hosting interconnected ecosystems influenced by anthropogenic disturbances and climate change (Ballut-Dajud *et al.*, 2022; Libonati *et al.*, 2020).

These wetlands are situated at altitudes ranging from 80 to 150 m, with predominantly low-permeability soils and strongly seasonal hydrological dynamics. According to Tomas *et al.* (2021), humid savanna formations are particularly vulnerable to fire due to the higher vegetation load maintained by flood-induced fertility, making these areas susceptible to burning during the dry season

Studies such as Viganó *et al.* (2017) report that, among the municipalities comprising the Pantanal, the one with the largest territorial extent is Corumbá (MS), covering approximately 65.000 km² and located within the Pantanal biome. A large portion of the original vegetation cover has been replaced by crops and pastures for extensive cattle ranching, promoting significant changes in land use and cover and, consequently, intensifying processes of environmental degradation and the occurrence of wildfires.

Since 2019, the biome has been experiencing a prolonged drought, peaking in 2020 and 2024, which has intensified natural disasters and contributed to a wildfire crisis (Mataveli *et al.*, 2021; Tomas *et al.*, 2021; Pereira *et al.*, 2024). This pattern can be observed in terms of annual burned area. According to MapBiomas (2024), in the Pantanal, the burned area in 2020, 2021, 2022, 2023, and 2024 was 25 893.83 km², 16 455.67 km², 2521.20 km², 6283.05 km², and 22 199.87 km², respectively. The value observed in 2024 represents an increase of approximately 253.3% compared to 2023.

Given this scenario, it is essential to develop more effective models for mapping and monitoring burned areas, aiming to mitigate the environmental impact of wildfires (Pazare *et al.*, 2022; Singh and Jeganathan, 2024).

Significant research has been conducted to improve both the faster and accuracy of fire detection and timely interventions (Priya and Vani, 2019; Cho *et al.*, 2023; Ghali and Akhloufi, 2023; Dadkhah *et al.*, 2025). This is because understanding fire occurrence patterns through remote sensing

 EISSN 1988-8740

allows the extraction of essential information for effective response and decision making during fire events (Dutra *et al.*, 2022; Mojica *et al.*, 2024; Lee *et al.*, 2025).

According to Md Jelas *et al.* (2024), the deep learning approach based on Convolutional Neural Networks (CNNs) in the field of remote sensing has primarily focused on fire hotspot detection, followed by the identification of deforestation and forest degradation processes.

These approaches have been employed using CNNs, integrating multispectral images, such as those from the Sentinel-2 sensor, particularly for the identification of vegetation suppression processes, segmentation of features associated with deforestation, and identification of areas affected by wildfires (Hu *et al.*, 2021; Wahab *et al.*, 2021)

Braga *et al.* (2025) used CNN architectures such as U-Net to segment degraded areas, including logging, fires, and road construction, in the Amazon within the Mato Grosso, Brazil. These studies demonstrated that the implemented REDD+AI model, based on CNNs, achieved higher overall accuracy (95.65% ± 1; 95% CI) compared to other widely used forest loss monitoring systems, such as DETER (87.40%), Tropical Moist Forest (86.77%), and Global Forest Change (86.55%) (Dalagnol *et al.*, 2023; Braga *et al.*, 2025). Authors such as Basu *et al.* (2015), and Hu *et al.* (2021) highlighted the advantage of using CNNs over traditional machine learning techniques.

Hu *et al.* (2021) compared CNN architectures and machine learning methods using Sentinel-2 images to segment areas affected by wildfires. The results showed that U-Net and HRNet achieved a mean Intersection over Union (mIoU) of 0.90 and a Kappa coefficient of 0.89 - 0.90, with omission and commission errors below 8%. In comparison, traditional models, such as Random Forest, reached a Kappa of 0.82, and individual spectral indices, such as the Normalized Burn Ratio (NBR), achieved 0.80.

This generalization capability has motivated the use of different CNN architectures in research focused on transfer learning for image classification and segmentation tasks (Guo *et al.*, 2016; Santiago Júnior, 2024). According to Yin *et al.* (2017), this approach has become a powerful tool for scene classification in remote sensing, particularly in contexts with limited availability of labeled data.

Recent advances in deep learning methods applied to remote sensing have revealed gaps caused by spectral, spatial, and radiometric differences between sensors. To address these limitations, studies such as those by Garcia *et al.* (2020), Saha *et al.* (2022), and Li *et al.* (2025) have shown that integrating information from multiple sensors each with distinct resolutions, spectral bands, and contextual attributes within a transfer learning framework can improve the generalization ability of deep learning models, even in the presence of substantial variability between the domains involved.

Although previous studies applying CNNs to remote sensing imagery (Zhou *et al.*, 2018; Santiago Júnior, 2024) have often relied on generic pretrained models, such as ImageNet, MNIST, or Kaggle datasets composed of RGB images of natural and urban objects, Priya and Vani (2019) highlight that spectral differences between conventional datasets and remote sensing data can limit model generalization.

However, despite the widespread application of different CNN architectures in computer vision tasks, typically using the datasets mentioned above, there remains, as discussed by Erhan *et al.* (2010), Simonyan and Zisserman (2015) and Yandouzi *et al.* (2022), a shortage of studies exploring remote sensing patterns using non-conventional imagery. Therefore, it is necessary to employ remote sensing data that enables the development of intra-domain deep learning models tailored to specific environmental contexts.

A significant gap is also identified in the literature regarding the use of intra-domain transfer learning approaches, as few studies evaluate models across datasets with similar spectral characteristics but originating from distinct biogeographical regions, particularly when adapting models trained in temperate environments (such as EuroSAT) to tropical biomes characterized by pronounced spatial and spectral heterogeneity, such as the Pantanal.

Given this context, it is assumed that models trained with data from temperate regions may, to some extent, contribute to advancing knowledge on transfer learning in tropical environments, which are largely composed of landscapes with high spatial and spectral heterogeneity. Studies such as this are believed to have the potential to expand our understanding of transfer learning across remote sensing imagery, especially at a critical moment when it is essential to deepen our comprehension of fire dynamics in tropical biomes.

## 2. Material and method

### 2.1. Study area

The study area is the Pantanal Biome, located in the center of South America within the Upper Paraguay River Basin. Covering approximately 138.183 km², 65% of its extent lies in the state of Mato Grosso do Sul and 35% in Mato Grosso (EMBRAPA, 2018). For this work, orbital image data were analyzed for the twelve Brazilian municipalities with the highest number of fire hotspots recorded between July 1, 2024, and September 19, 2024. In Mato Grosso, the municipalities analyzed were Cáceres, Barão de Melgaço, Santo Antônio do Leverger, Poconé, and Nossa Senhora do Livramento. In Mato Grosso do Sul, the cities included in the analysis were Corumbá, Aquidauana, Miranda, Porto Murtinho, Ladário, Sonora, and Coxim (Figure 1).

### 2.2. Data collection

The data preparation workflow began with the Pantanal dataset, using the Google Earth Engine platform (Gorelick *et al.*, 2017). For filtering images from the fire season, Sentinel-2 imagery at the Level-2A (Surface Reflectance) processing level was used, covering the period from June to September 2024, with a cloud cover filter of less than 20%.

The Red (B4), Near-Infrared (B8), and Shortwave Infrared (B11) spectral bands were selected. Since band B11 has a spatial resolution of 20 m, it was

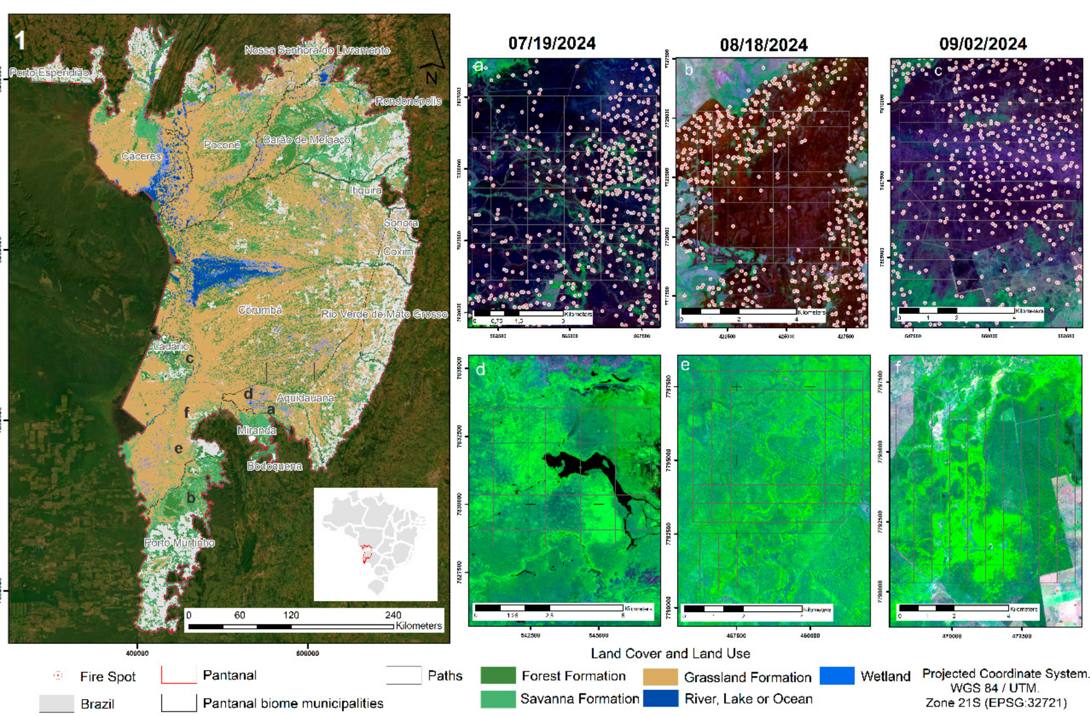


**Figure 1.** Location map of the study area. Pantanal region with the location of the grid maps displayed on the right. Panels a to c present examples of burned areas: in Aquidauana (July), Porto Murtinho (August), and Corumbá (September), respectively. Panels d to f show examples of unburned areas: in Aquidauana (July), and in Corumbá during August and September, respectively.

resampled to 10 m using bilinear interpolation, ensuring spatial consistency among the bands.

From these bands, the spectral indices NDVI [(B8 − B4) / (B8 + B4)] and NBR [(B8 − B11) / (B8 + B11)] were calculated. These indices are widely used for burned-area monitoring (Alcaras *et al.*, 2022; Mataveli et al., 2021), where high values indicate healthy vegetation and low values indicate burned areas or exposed soil (Unnikrishnan & Reddy, 2020; Simioni *et al.*, 2022).

A total of 2078 tiles of 64×64 pixels were generated (Figure 1), capturing the variability of fire events, including both affected and non-affected areas. These tiles were used both in pre-training (model from scratch) and fine-tuning. For area selection, fire hotspots reported by INPE between June and September 2024 were considered. Of this total, 1040 patches correspond to burned areas and 1038 to non-burned areas, indicating an almost perfectly balanced distribution between classes.

The next step consisted of the preparation of the EuroSAT dataset, composed of 27 000 tiles of Sentinel-2A MSI images (ESA, 2025), with a size of 64×64 pixels and 13 bands, featuring spatial resolutions of 10 m, 20 m, and 60 m, distributed across 10 land-cover classes (Helber *et al.*, 2019). In the EuroSAT dataset, two specific classes were selected: herbaceous vegetation, with 2000 samples, and pasture, with 2000 samples, aiming to increase spectral variability and improve the models' generalization capability.

## 2.3. Experimental model: training the model from scratch

The VGG-19 architecture was used, consisting of 16 convolutional layers and 3 fully connected layers, grouped into 5 blocks, totaling 19 trainable layers (Simonyan and Zisserman, 2015). For the experimental training, the CNN input was adapted to receive 5 spectral channels, corresponding to the data structure of the EuroSAT and Pantanal datasets: B4-Red, B8-NIR, B11-SWIR, NDVI, and NBR. Additionally, the number of filters in each convolutional layer was reduced, while maintaining 3×3 kernels, max-pooling with a stride of (2,2), and the ReLU activation function (Krizhevsky *et al.*, 2012; Guo *et al.*, 2016), as shown in Figure 2.

Initially, the model was trained using the original number of neurons in the fully connected layer, which resulted in overfitting. This behavior is associated with the high complexity of the VGG-19 architecture relative to the size of the dataset, as VGG-19 was originally trained on large-scale datasets such as ImageNet (Simonyan and Zisserman, 2015).

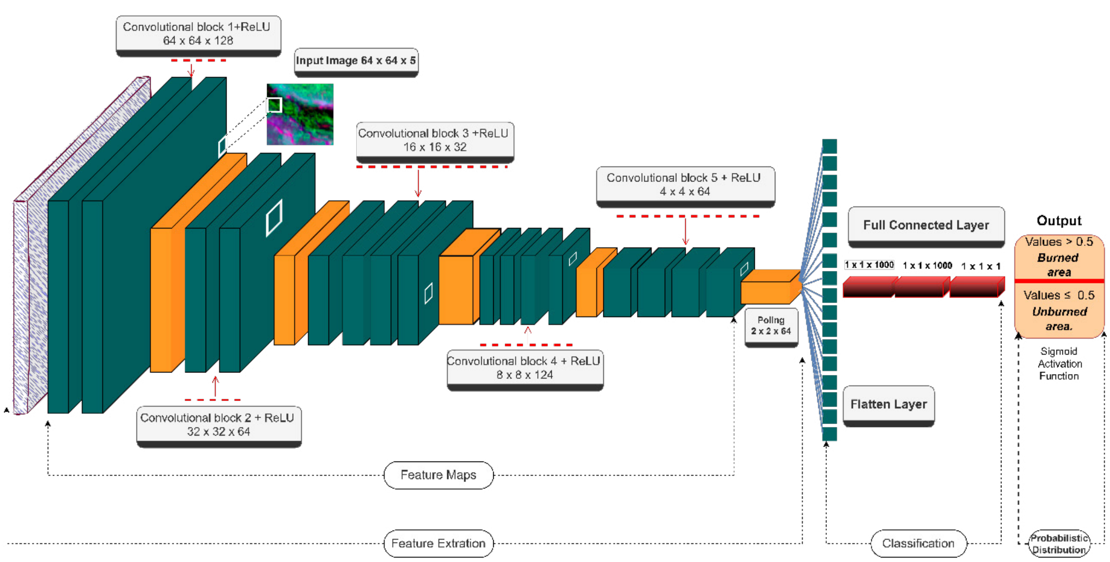


**Figure 2.** Modified VGG-19 architecture trained from scratch on the EuroSAT and Pantanal Biome datasets.

To mitigate this effect, multiple configurations with a progressive reduction in the number of neurons were evaluated. The configuration with 1000 neurons yielded comparable validation performance, while reducing overfitting and improving generalization.

In this study, the fully connected layer of VGG-19 was modified to contain 1000 neurons each, instead of 4096, reducing the model's complexity. In the output layer, a sigmoid activation function was used to convert the predictions into probabilities ranging from 0 to 1. All VGG-19 adaptations were implemented using TensorFlow (version 2.13), with the Keras API, enabling the CNN to be adjusted to the objectives of this study (Huang *et al.*, 2017).

Once the VGG19 architecture was adapted, 4000 tiles from classes 0 (herbaceous vegetation) and 1 (pastures) of the EuroSAT dataset were used for training and validation, configuring the CNN to receive five channels. The choice of these classes was based on the expectation that their phytovegetation characteristics could enhance learning in the initial layers of VGG-19, since, due to the limited number of samples in the Pantanal dataset, spectral and spatial patterns might not be captured. In this context, intra-domain transfer is expected to provide generalization of burned areas within the environmental context of the Pantanal.

## 2.4. Pre-training and transfer learning with fine-tuning

After the pre-training performed on EuroSAT, it was necessary to adapt the CNN input to five channels. In other words, the same number of channels used in the EuroSAT model training was maintained, ensuring consistency between the two stages of the process. This adaptation is essential to analyze the extent to which the transfer of knowledge between different bands and spectral characteristics contributes to improving scene classification performance in the Pantanal context.

Figure 3 shows the frozen blocks, whose weights remained unchanged, as well as the last two blocks, whose weights were adjusted based on the new data from the Pantanal dataset.

In both the Experimental Training and fine-tuning models, the loss function used was Binary Cross Entropy (Chollet, 2017) as defined in Equation (1), to measure the discrepancy between predicted and actual values, defining the loss function. This method, widely applied in binary classification tasks, was used with batches of 16 and 32 samples during error backpropagation. For this process,

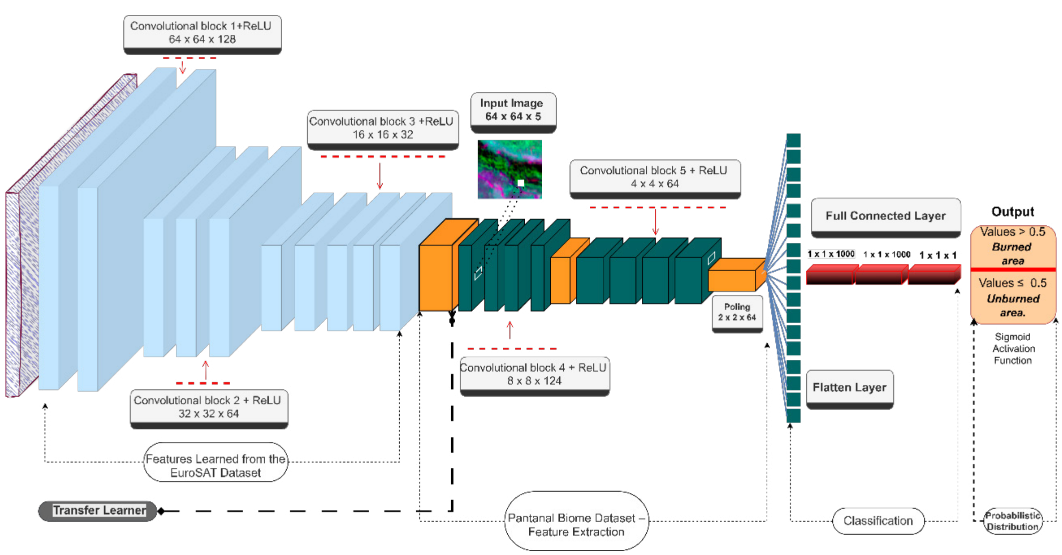


**Figure 3.** Modified VGG-19 architecture showing frozen layers pretrained on the EuroSAT dataset (in blue) and trainable layers fine-tuned on the Pantanal dataset.

 EISSN 1988-8740

the Root Mean Square Propagation (RMSprop) optimizer (Hinton *et al.*, 2012) and Adaptive Moment Estimation (Adam) (Kingma & Ba, 2015) were employed.

$$l = \sum_{i=1}^{n} \left[ y_{\mathrm{i}} \cdot log(\hat{y}_{\mathrm{i}}) + (1 - y_{\mathrm{i}}) \cdot \log(1 - \hat{y}_i) \right] \quad (1)$$

Where $N$ is the total number of images used for training, $y$ is the true class label, $\hat{y}$ is the predicted value after sigmoid activation (probability of being class 1), and *log* denotes the natural logarithm.

To ensure greater stability in model optimization, learning rates of 1e-3and 1e-4 were used, dynamically adjusted by *Keras/TensorFlow ReduceLROnPlateau* function, which halves the learning rate after 5 epochs without improvement in the validation loss, with a minimum limit of 1e-6. To reduce gradient instability and overfitting, L2 regularization (1e-4) was applied to the convolutional and dense layers (Goodfellow *et al.*, 2016), along with dropout rates of 30% and 50% in the fully connected layers (Srivastava *et al.*, 2014). The experiments were conducted on a server with an Intel Core i5-10210U processor (1.60–2.11 GHz), 8 GB of RAM, and a 64-bit operating system. This configuration ensured not only the selection of the best model for fine-tuning but also that the generalization on the Pantanal dataset achieved the best performance on the test data.

## 2.5. Training and testing dataset division

Given the large number of images (4000), we split the dataset into 70% for training and 30% for validation/test using the Holdout method (Random Resampling), which ensured good representativeness of the herbaceous vegetation and pasture classes.

On the other hand, for the transfer learning of VGG-19 on the Pantanal dataset, *cross-validation* was applied (Pérez *et al.*, 2021; Alkan *et al.*, 2024). The dataset was split into 80% for training/validation and 20% (416 images) for testing. The 1662 images allocated for training/validation were organized into 5 folds. In each iteration, one fold was used as the validation set, while the remaining four folds were used for training. At the end of the five iterations, the mean and standard deviation of the metrics were calculated, enabling a robust evaluation of the model and the identification of the parameters with the best performance.

## 2.6. Data augmentation

The data augmentation technique was applied (Dosovitskiy *et al.*, 2015) to increase the variety of images during the training of the VGG-19. For this purpose, synthetic images were dynamically generated during training with two types of transformations: random horizontal flips and random rotations of the original images, which allowed for an increased effective dataset size. This technique was specifically applied to transfer learning with a fine-tuning model due to the limited number of images available in the Pantanal dataset.

## 2.7. Evaluation metrics

Model validation was conducted using metrics such as overall accuracy, defined as the number of correct predictions in each category divided by the total number of observations (Dong *et al.*, 2022), as well as F1 score, precision, and recall. These metrics were calculated based on True Positives (TP), True Negatives (TN), False Positives (FP), and False Negatives (FN), which are the elements of the confusion matrix.

## 2.8. SHAP (Shapley Additive Explanations) value contributions

This stage consisted of interpreting the decisions made by the models in order to identify the most relevant bands in the dataset for the prediction task in the Pantanal dataset. For this purpose, SHAP values (Shapley Additive Explanations) were calculated, representing the degree of contribution of each spectral band used in the models and allowing the identification of the most important features for prediction (Lundberg & Lee, 2017). Positive values indicate that the band increases the probability of predicting class 1, while negative values reduce that probability, being associated with class 0. Thus, this approach was adopted to enhance the explainability of the tested models, providing a more solid understanding of the attributes that influenced the prediction decisions.

**Table 1.** Model performance evaluation during Experimental Training using the Holdout method with the EuroSAT dataset. The *RMSprop* optimizer with 50 epochs achieved a validation loss of 0.202 and a validation accuracy of 0.938.

| ReLu activation function RMSprop optimizer | | | | Best model performance | | |
|---|---|---|---|---|---|---|
| Learning rate | Epochs | Batch size | Dropout dense layers | Val acc | Val loss | Acc global test |
| 0.001 | 50 | 32 | 0.1 | 0.925 | 0.207 | 0.939 |
| 0.0001 | 100 | 32 | 0.1 | 0.931 | 0.320 | 0.919 |
| **0.001** | **50** | **32** | **0.5** | **0.938** | **0.202** | **0.942** |
| 0.001 | 100 | 32 | 0.5 | 0.939 | 0.239 | 0.929 |
| 0.0001 | 100 | 32 | 0.3 | 0.929 | 0.518 | 0.922 |
| ReLu activation function Adam optimizer | | | | Best model performance | | |
| 0.001 | 50 | 32 | 0.1 | 0.931 | 0.207 | 0.932 |
| 0.0001 | 100 | 32 | 0.3 | 0.922 | 0.229 | 0.939 |
| 0.001 | 50 | 32 | 0.5 | 0.505 | 0.705 | 0.532 |
| 0.001 | 100 | 32 | 0.5 | 0.520 | 0.793 | 0.543 |
| 0.0001 | 100 | 32 | 0.3 | 0.921 | 0.333 | 0.921 |

## 3. Results

### 3.1. Experimental training model with the EuroSAT dataset

The results of the VGG-19 simulations using the EuroSAT dataset are presented in Table 1. For the training and weight optimization process, a total of 5 991 629 parameters were processed. The highest accuracy achieved was 0.942 for the model using the *RMSprop* optimizer and 0.939 for the model using the *Adam* optimizer, with losses of 0.202 and 0.229, respectively. Initially, the model was trained for 25 epochs, but it did not achieve satisfactory performance. Subsequently, model training was extended to 100 epochs, but overfitting was observed. These analyses showed that the best-trained model converged before 50 epochs.

Thus, the model selected for pre-training and transfer learning on the Pantanal dataset was the one using the RMSprop optimizer for 50 epochs, with a loss of 0.202 (Figure 4), representing the best-performing model in terms of generalization on the test data.

In Figure 4, both the loss and validation loss curves show a consistent decline, reaching values of 0.1 and 0.2, respectively, converging before epoch 50.

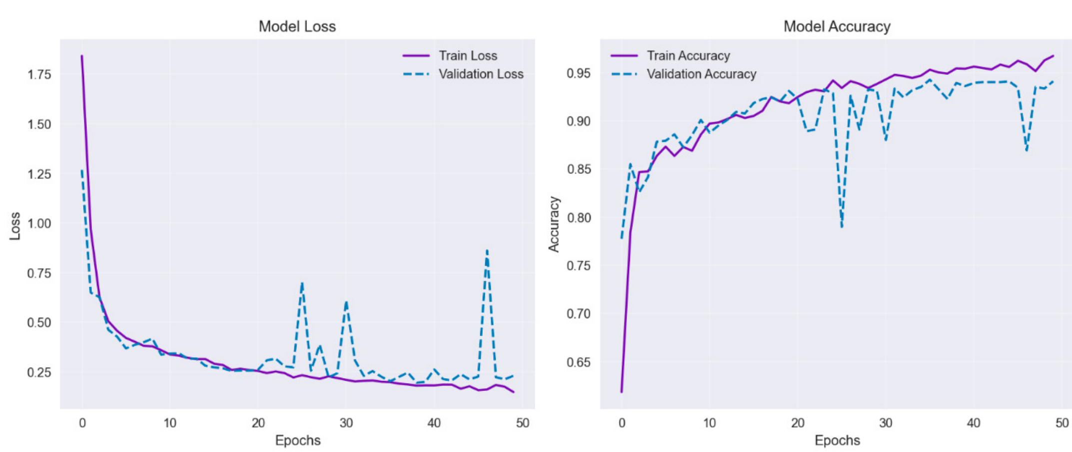


**Figure 4.** Evolution of the Loss and Accuracy curves during training and validation of the Experimental Training model, using the *RMSprop* optimizer and 50 epochs, with the EuroSAT dataset. Model selected for fine-tuning.

**Table 2.** Model performance evaluation during transfer learning: fine-tuning using *K-Fold* cross-validation with the Pantanal dataset.

| ReLU activation function Adam optimizer | | | | 5-fold CV-Average ± Standard deviation of training and validation performance | | Best model performance | | |
|---|---|---|---|---|---|---|---|---|
| Learnig rate | Epochs | Bathsize | Dropout dense layers | Avg. val. acc | Avg. val. loss | **Val acc** | **Val loss** | Acc global test |
| **0.0001** | **50** | **16** | **0.5** | **0.892± 0.099** | **0.655±0.095** | **0.96** | **0.15** | **0.95** |
| 0.001 | 100 | 16 | 0.3 | 0.885± 0.120 | 0.650±1.119 | 0.96 | 0.23 | 0.94 |
| 0.0001 | 50 | 32 | 0.5 | 0.815± 0.171 | 1.583± 1.693 | 0.97 | 0.16 | 0.94 |
| 0.001 | 100 | 32 | 0.3 | 0.581±0.130 | 0.635±0.123 | 0.83 | 0.39 | 0.80 |
| ReLU activation function RMSprop optimizer | | | | 5-fold CV-Average ± Standard deviation of training and validation performance | | Best model performance | | |
| 0.0001 | 50 | 16 | 0.5 | 0.791± 0.197 | 3.030± 2.184 | 0.94 | 0.31 | 0.94 |
| 0.001 | 100 | 16 | 0.3 | 0.771±0.156 | 2.994± 2.141 | 0.95 | 0.21 | 0.95 |
| 0.0001 | 50 | 32 | 0.5 | 0.696± 0.208 | 3.261± 2.228 | 0.95 | 0.51 | 0.93 |
| 0.001 | 100 | 32 | 0.3 | 0.632± 0.162 | 4.099± 1.948 | 0.94 | 0.20 | 0.91 |

Although the training accuracy continued to increase, reaching values close to 0.96, the epoch at which the validation accuracy achieved the highest generalization performance on the test data was selected, resulting in an overall accuracy of 0.942.

## 3.2. Transfer learning: fine-tuning using the Pantanal dataset

After pre-training the VGG-19 architecture on the EuroSAT dataset and saving the best model from 50 epochs using the *RMSprop* optimizer, transfer learning was performed using the dataset of areas affected by fires in the Pantanal biome in 2024.

Table 2 presents the results, highlighting that the best performance was achieved with the ReLU activation function, Adam optimizer, learning rate of 1e-4, and batch size of 16. This selection is accompanied by the overall test accuracy metric, which evaluates the model's generalization on the test data.

In Figure 5, it can be observed that the training and validation loss curves converge and stabilize

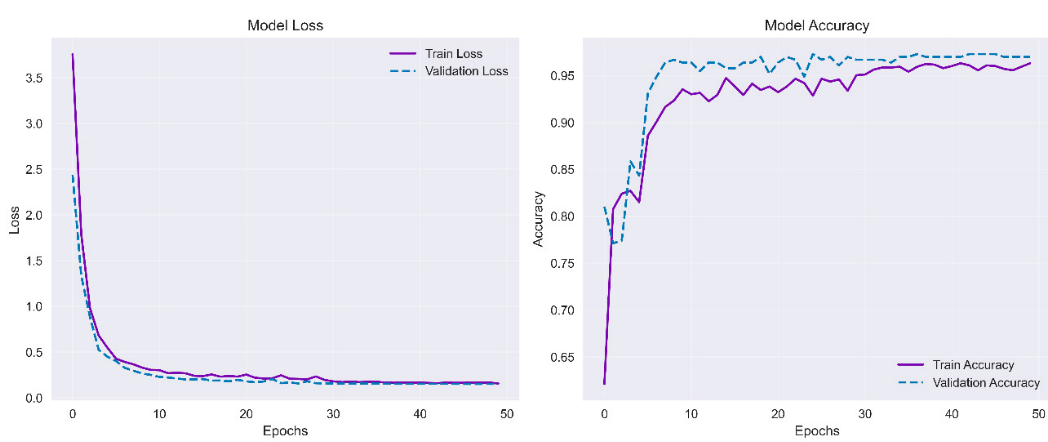


**Figure 5.** Evolution of the Loss and Accuracy curves during transfer learning: fine-tuning using the *Adam* optimizer over 50 epochs and a learning rate of 0.0001 with the Pantanal dataset. This model was then used to generate predictions and assess generalization on the test dataset.

around 0.160, with an overlap between both curves throughout the epochs. This behavior indicates the absence of overfitting and a balance between learning and generalization, demonstrating a high learning efficiency, as the low loss values indicate predictions close to the true values.

Regarding accuracy, the validation data initially show higher accuracy than the training data up to epoch 10. From epoch 20 onward, however, training accuracy surpasses validation accuracy, reaching approximately 0.960, while validation accuracy stabilizes around 0.95. These results correspond to an overall accuracy of 95.4%, indicating that the model is capable of correctly predicting 95% of the data, both for seen and unseen instances during training.

## 3.3. Training the model from scratch using the Pantanal Dataset

Following the research objective of evaluating model performance under different conditions, the model was trained from scratch, without pre-trained weights, using the Pantanal dataset. For this purpose, two types of real-time data augmentation were applied during the training process (Figure 6).

Thus, the modified VGG-19 was trained with 2.078 tiles from the Pantanal dataset, with data augmentation applied to each batch. In the first model with 50 epochs, approximately 311.700 augmented images were generated, resulting from multiplying the total number of images in the training set by the number of iterations in each k-fold. Figure 6 illustrates examples of some of the augmented training image variations.

In Table 3, it can be observed that the *Adam* model, with a learning rate of 0.0001, 50 epochs, and a batch size of 16, achieved strong performance in validation loss, providing the best model for classifying burned and unburned areas, with a loss value of 0.007. The model reached a global test accuracy of 0.97, representing one of the highest-performing models among those evaluated.

By examining the learning curve of the *Adam* model (Figure 7), epoch 38 stands out, where the validation accuracy surpassed 95%. The loss behavior was similar for both models; however, loss stabilization occurred before epoch 30, unlike the *RMSprop* model, which stabilized after epoch 40.

Although the *RMSprop* model, with a learning rate of 0.0001 and 50 epochs, achieved a minimum validation loss of 0.0976, it was not selected for the generalization stage on the test set. This is because the standard deviation observed during cross-validation indicated higher variability across folds, resulting in lower model stability.

## 3.4. Comparative analysis of the results of the application to test data

Results from the test data evaluation metrics are detailed in Table 4. The class defined as unburned

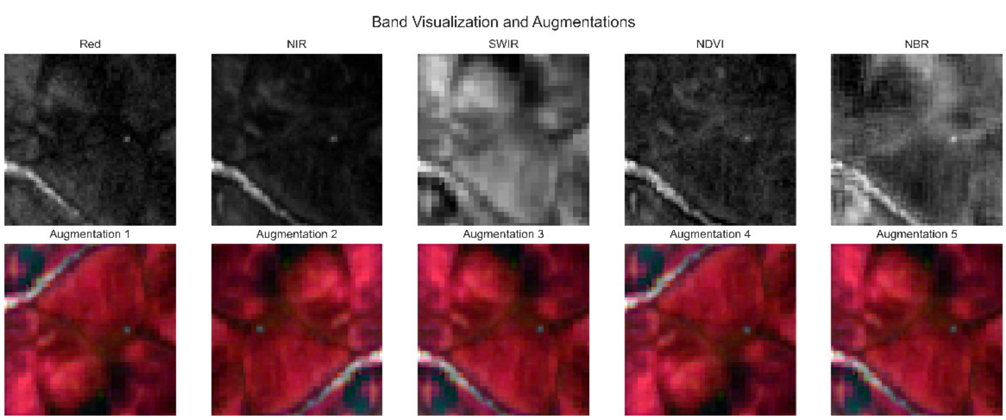


**Figure 6.** Application of data augmentation using random horizontal flip and random rotation on a burned area image, used for training a VGG-19 model without pre-trained weights (from scratch). Sentinel-2 image composition: SWIR–NIR–Red.

 EISSN 1988-8740

**Table 3.** Model performance evaluation during training on the Pantanal dataset without pre-trained weights, using K-Fold cross-validation.

| ReLU activation function Adam optimizer | | | | 5-fold CV - Average ± standard deviation of training and validation Performance | | Best model performance | | |
|---|---|---|---|---|---|---|---|---|
| Learning rate | Epochs | Bath size | Dropout dense layers | Avg. val. acc | Avg. val. loss | Val acc | **Val loss** | Acc global test |
| **0.0001** | **50** | **16** | **0.5** | **0.851± 0.138** | **0.282± 0.122** | **0.98** | **0.07** | **0.97** |
| 0.001 | 100 | 16 | 0.3 | 0.693± 0.003 | 0.913± 0.431 | 0.50 | 0.69 | 0.50 |
| 0.0001 | 50 | 32 | 0.5 | 0.772± 0.166 | 0.404± 0.271 | 0.95 | 0.09 | 0.95 |
| 0.001 | 100 | 32 | 0.3 | 0.500± 0.001 | 0.989± 0.583 | 0.50 | 0.69 | 0.49 |
| ReLU activation function RMSprop optimizer | | | | 5-fold CV - Average ± standard deviation of training and validation performance | | Best model performance | | |
| 0.0001 | 50 | 16 | 0.5 | 0.746± 0.192 | 0.476± 0.336 | 0.97 | 0.09 | 0.96 |
| 0.01 | 100 | 16 | 0.3 | 0.500± 0.001 | 0.707± 0.018 | 0.50 | 0.69 | 0.52 |
| 0.0001 | 50 | 32 | 0.5 | 0.695± 0.230 | 0.550± 0.385 | 0.97 | 0.08 | 0.96 |
| 0.01 | 100 | 32 | 0.3 | 0.500± 0.016 | 0.714± 0.026 | 0.50 | 0.69 | 0.50 |

exhibited high precision, reflecting a large proportion of correctly classified observations (0.89 % and 0.96%, respectively). The model without pre-trained weights achieved slightly higher performance, with an overall accuracy of 96.6%.

In the error matrix (Figure 8), it can be observed that the unburned class showed greater confusion in the classification in both models, possibly due to the well-known difficulty of distinguishing spectral patterns of vegetation in wetland areas and in areas degraded by fires (Sausen, 2007; Silva *et al.*, 2021; Mataveli *et al.*, 2021). Only the test data were used, totaling 416 tiles, that is, data the model had never seen during training.

## 3.5. SHAP value contributions

In Figures 9a and 9b, the contributions of each band to the classification model are shown in relation to the model's average prediction. Positive patterns, represented in red, indicate an increase in the probability that an image is classified as class 1 (burned area). It is evident that the NIR and NBR indices contribute positively to increasing the probability of this class. Conversely, SHAP values represented in blue show that the NDVI band

a

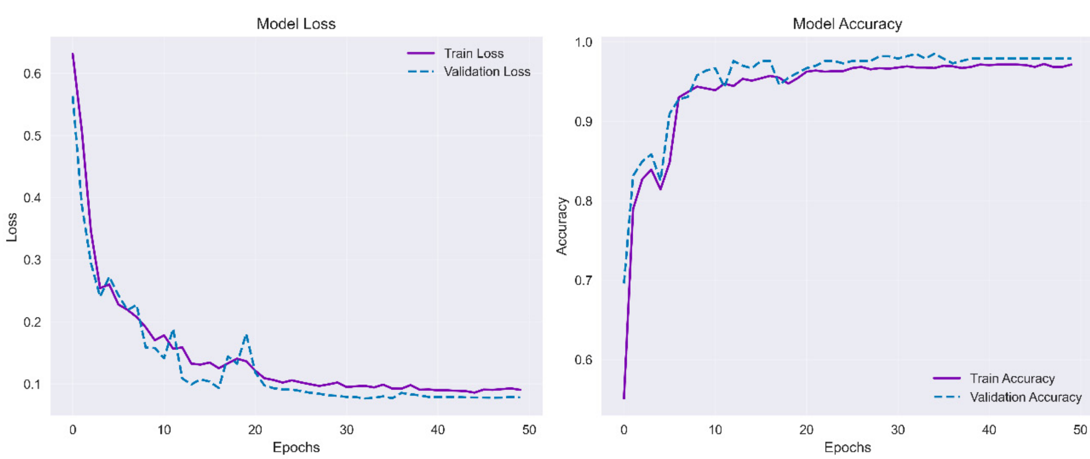


**Figure 7.** Evolution of the Loss and Accuracy curves during training without pre trained weights, using the Pantanal dataset. The model was trained with the *Adam* optimizer over 50 epochs and a learning rate of 0.0001. This model was then used to generate predictions and assess generalization on the test dataset.

**Table 4.** Performance comparison between transfer learning and without pre-trained weights on the test set using Pantanal data.

| Best model performance transfer learning (fine-tuning) | | | | |
|---|---|---|---|---|
| | | Precision | Recall | F1-Score |
| Unburned area | | 0,89 | 0.96 | 0.92 |
| Burned area | | 0.95 | 0.88 | 0.92 |
| accuracy | 95.4% | | | |
| **Best model performance VGG-19 raining the model from scratch** | | | | |
| | | Precision | Recall | F1-Score |
| Unburned area | | 0.96 | 0.98 | 0.97 |
| Burned area | | 0.98 | 0.96 | 0.97 |
| accuracy | 96.6% | | | |

reduced the probability of classification as class 1, indicating a strong, but negative, influence that favors the prediction of class 0 (unburned area).

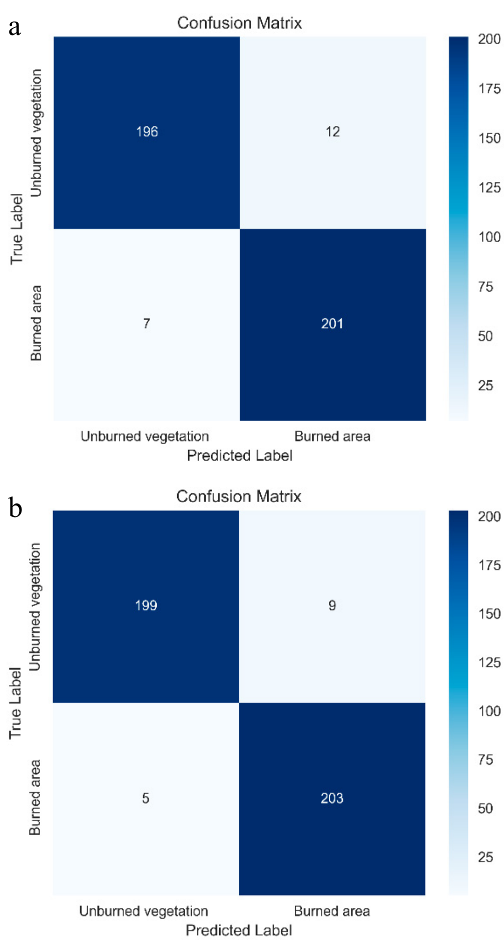


**Figure 8.** (a) Error matrix of the best model performance using transfer learning (b) Error matrix of the best CNN model performance without pre-defined parameters.

The spectral characteristics of the bands for identifying burned areas in this study are primarily related to NIR and NBR, with a smaller contribution from the SWIR band. This demonstrates that the models learned specific patterns in the spectral features of these bands. For example, the NIR band exhibits low reflectance in burned areas due to vegetation loss, making it a relevant feature for class 1. Similarly, low spectral values in the NBR index are typical of burned areas, reinforcing its relevance for this class.

## 4. Discussion

Although the model from scratch presented slightly superior performance in terms of validation loss (0.07 compared to 0.15) and test accuracy (0.97 compared to 0.95), this difference can be considered marginal. This is because the transfer learning-based model demonstrated faster convergence and competitive validation accuracy (0.892±0.099), higher than that of the model from scratch (0.851±0.138), indicating a more stable learning process.

This result reinforces the findings of Erhan *et al.* (2010), who showed that pre-training acts as a form of regularization by providing better weight initialization, thereby favoring the generalization process. In the present study, this behavior was reflected in the faster convergence of the training and validation loss curves (Figure 5), observed before the 10th epoch, indicating a more stable learning process with lower susceptibility to overfitting.

The results indicate that both approaches presented competitive performance. Although the model from scratch achieved slightly higher test

 EISSN 1988-8740

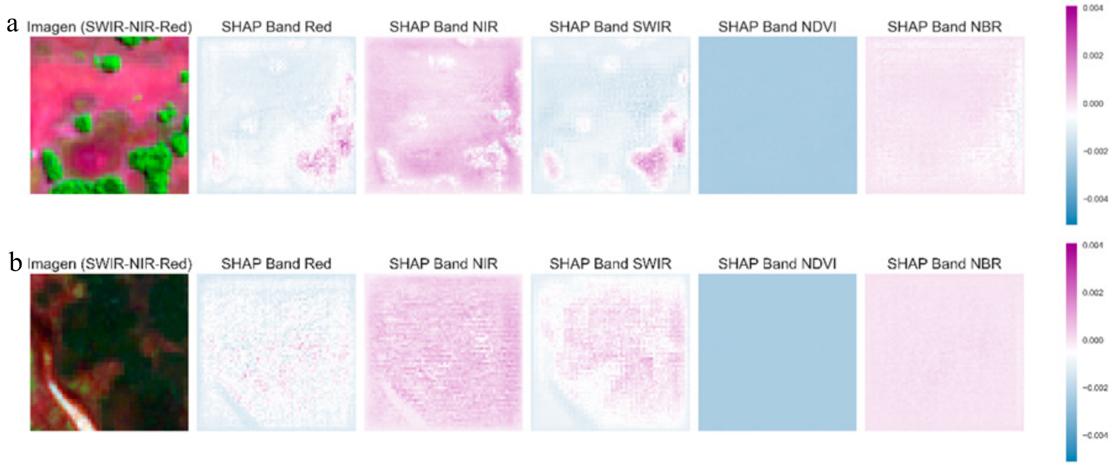


**Figure 9.** Band-wise contributions of SHAP values. (a-b) Positive SHAP values (in pink) increase the probability of class 1 (burned area), while negative values (in blue) decrease it, thus contributing to class 0 (unburned area).

accuracy and greater implementation simplicity, the approach demonstrated greater stability to hyperparameter variations and faster convergence, as evidenced by the training and validation loss curves, making this methodology useful in intra-domain scenarios and contributing to classification tasks in contexts with limited data availability in remote sensing. This behavior is consistent with Simonyan and Zisserman (2015), who demonstrate the effectiveness of deep architectures and the benefits of transfer learning in computer vision tasks

As discussed earlier, the use of unconventional images, such as those from the Pantanal and the application of transfer learning, allows the exploration of spatial and spectral patterns specific to this biome. In Figure 10, it is observed that the model without pre-trained parameters was able to correctly identify burned areas, showing contrast between them and exposed soil (dark and reddish tones). Although it is known that red and SWIR increase and NBR decreases after fire (Sacramento *et al.*, 2020), the results demonstrate that the model reliably captured spectral variations, ensuring the distinction between healthy vegetation and burned areas in the NDVI and NBR indices.

In Figure 11, we present excerpts of areas correctly classified as non-burned using the transfer learning model. A contrast can be observed between herbaceous vegetation (light green) and flooded areas (purple and black tones). This highlights that the model was able to correctly classify flooded herbaceous wetland areas.

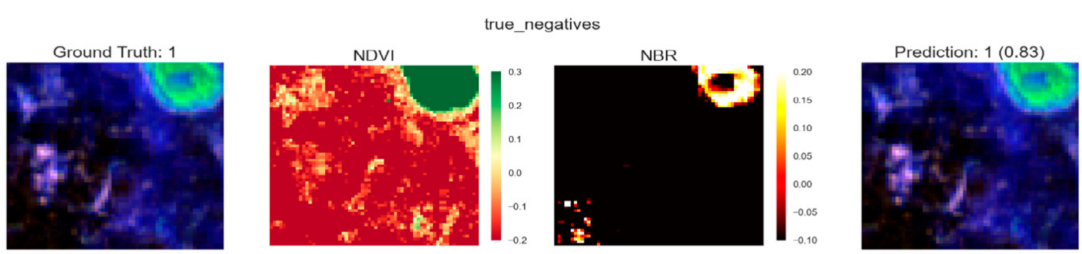


**Figure 10.** True Negative. Patterns of areas affected by fires in wetlands, identified using a VGG-19 model trained from scratch. Municipality of Corumbá, September 2, 2024. RGB composition: SWIR, NIR, and Red (Sentinel-2).

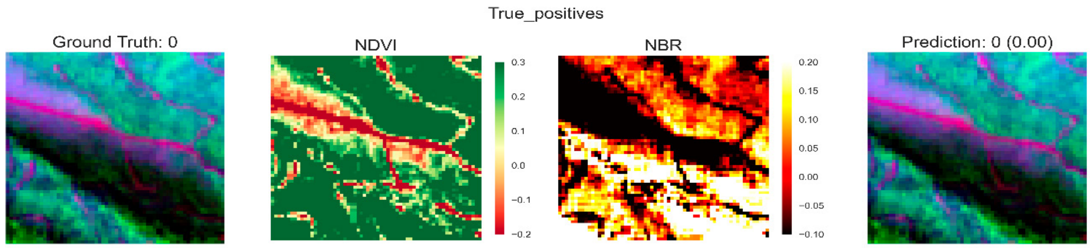


**Figure 11.** True positive. Transfer learning model. Patterns of wetland grassland areas not affected by fires in the Pantanal Biome, in the municipality of Aquidauana, on July 19, 2024. Sentinel-2. RGB composition: SWIR, NIR, and Red, Sentinel-2. The contrast between herbaceous vegetation (light green color) and flooded wetland areas (shades of purple and black) is evident.

It is noteworthy that in Figure 11, areas with higher organic matter content (magenta to purple tones) and herbaceous vegetation with saturated soils (a mixture of purple and green tones) can be observed. According to Sausen (2007), Gitelson *et al.* (2008), and Klemas (2011), the spectral response in wetland environments is strongly influenced by the mixture of water, suspended sediments, dissolved organic matter, and emergent vegetation. This complexity intensifies the confusion between classes with similar spectral signatures, as in this case, approaching the spectral response of exposed soil and burned areas.

In this sense, the observed patterns are consistent with a well-established spectral behavior described in the literature, which supports the interpretation of the classes identified in this study. However, this spectral similarity also represents an inherent limitation of the analysis, as it reduces the spectral separability between classes, potentially leading to ambiguities in distinguishing between burned and unburned areas, even in CNNs, especially in complex wetland environments.

This similarity in spectral behavior resulted in some misclassifications in the predictions, as shown in Figures 12 and 13. According to Shimabukuro and Smith (1991) and Mataveli *et al.*, 2021), this occurs frequently, even in deep learning models, due to the nature of the imaged targets. Based on the confusion matrices presented in Figure 8 (416 tiles per model), the transfer learning model achieved an overall accuracy of 95.43%, with 397 correct classifications and 19 errors.

The unburned vegetation class reached 47.12% (196 tiles) of correct classifications and 2.88% (12 tiles) of errors, while the burned area class achieved 48.32% (201 tiles) of correct classifications and 1.68% (7 tiles) of errors. The CNN model from scratch obtained an overall accuracy of 96.63%, with 402 correct classifications and 14 errors. The unburned vegetation class achieved 47.84% (199 tiles) of correct classifications and 2.16% (9 tiles) of errors, while the burned area class reached 48.80%

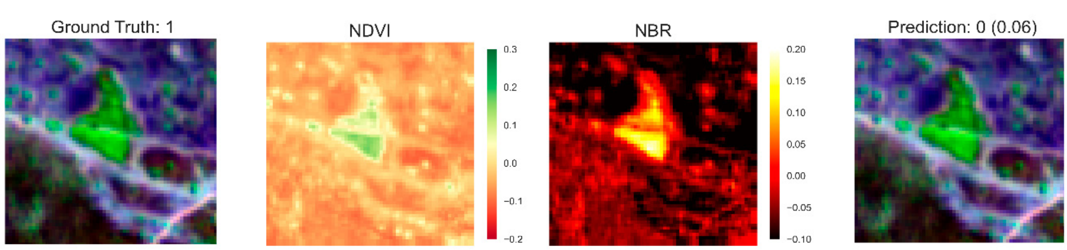


**Figure 12.** False negative. VGG19 transfer learning Model. Patterns of burned areas after wildfires in wetlands and exposed soil (darker areas) in the municipality of Aquidauana, on September 2, 2024. Sentinel-2. The composition highlights the spectral differentiation between burned areas (purple) and exposed soil (dark violet).

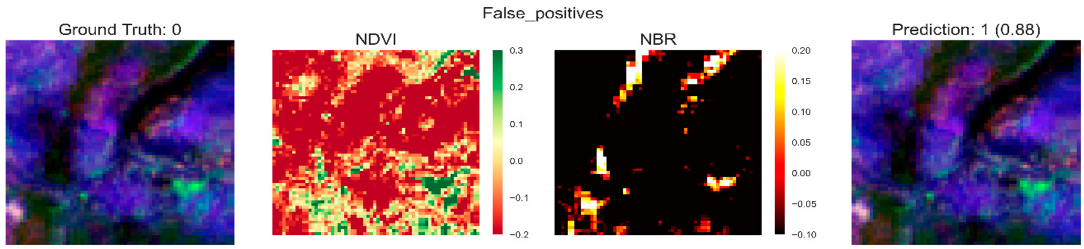


**Figure 13.** False positive. VGG-19 fine-tuning Model: Wetland areas not affected by fires mistakenly classified by the model as burned areas in the Pantanal biome, in the municipality of Corumbá, on September 2, 2024. RGB composition: SWIR, NIR, and Red, Sentinel-2.

(203 tiles) of correct classifications and 1.20% (5 tiles) of errors.

Priya & Vani (2019) demonstrated that transfer learning with pre-trained weights on ImageNet achieved 93% training accuracy and 92% test accuracy using the Inception-v3 architecture to classify fire and non-fire areas in WorldView satellite imagery. In the present study, the results obtained with transfer learning (95.43%) and with the CNN trained from scratch (96.63%) outperformed those reported by these authors, which can be attributed, in part, to the larger size of the dataset used, with 2078 tiles and a balanced distribution between classes: 1038 non-burned areas and 1040 burned areas, in comparison with the dataset used in that study, which included 239 fire samples and 295 non-fire samples. This result reinforces the validity of the present study, as the similarity between the source and target domains is a relevant factor that should be considered in the application of transfer learning in remote sensing.

In relation to Yandouzi *et al.* (2022), who reported 99.94% accuracy using ResNet50 for active fire detection, our results are approximately 3 percentage points lower. However, this difference should be contextualized, as the aforementioned study focused on the detection of active fire, namely flames and smoke in high-resolution drone and airborne imagery, whereas the present study classifies burned areas in satellite images. Cho *et al.* (2023) reported overall accuracy between 99.0 - 99.7% and F1-scores of 0.883 - 0.939 for burned area mapping using U-Net and *PlanetScope* imagery. Our results (95-96%) are slightly lower, and this difference can be explained by two main factors. First, the authors used the U-Net architecture, designed for semantic segmentation, whereas in this study, tile-based binary classifiers were employed. Second, the PlanetScope imagery used has a spatial resolution of 3 meters, while our data have a coarser resolution of 10 meters, which may have reduced the ability to capture fine details at the edges of burned areas and small fire patches.

As highlighted in the work of Hu *et al.* (2021), intra-domain transfer learning can be performed between Sentinel 2 imagery for semantic segmentation and directly applied to Landsat-8 data to segment burned and unburned areas using CNNs. Among the architectures tested, HRNet showed the best generalization capability, achieving a *Kappa* coefficient of approximately 0.9. Although the present study focused on tile-based binary classification, the proposed approach achieved 95.4% accuracy, which is consistent with findings from this line of research, since intra-domain knowledge transfer, even when applied to different tasks such as classification and segmentation, remains a relevant factor for success in remote sensing applications. Therefore, this aspect can continue to be explored in future studies, highlighting the advantages of this methodology.

## 5. Conclusions

The present research demonstrated that the application of the VGG-19 architecture shows high efficiency in classifying burned and unburned areas in the Pantanal biome, with satisfactory results achieved both through the transfer learning strategy and through training the model from scratch.

The transfer learning technique, with fine-tuning based on images from the EuroSAT dataset, achieved an accuracy of 95% in the classification of the Pantanal test data. In contrast, the training performed without pre-trained weights, using only the biome's own data, obtained superior performance with an overall accuracy of 96%, evidencing the model's ability to learn spectral patterns specific to the local vegetation.

These results indicate that the intra-domain transfer learning approach can be successfully applied to environmental monitoring in complex regions such as the Pantanal. However, the model trained from scratch achieved higher accuracy, suggesting that, in this case, training a CNN using local data allows for a better representation of region-specific spectral patterns.

Despite the high accuracy levels, the spectral similarity between wetland areas and burned areas resulted in classification errors, especially in the unburned class. This overlap in spectral responses is noted in the literature as a recurring challenge in floodplain ecosystems, such as the Pantanal, and reinforces the need for post-processing strategies or integration with other data sources.

Finally, the methodology employed in this study can be replicated in areas with complex ecological contexts, such as the Pantanal or other biomes characterized by high heterogeneity of land cover, flood seasonality, and aquatic vegetation dynamics. It also provides evidence regarding the applicability of these techniques in ecologically relevant regions, something that previous studies had not yet explored.

### Authors' contributions

Pastrana-Mojica, Fraga-Belloli and Boelter-Herrmann contributed to the conceptualization of the study, methodological design, development of the deep learning model, and final approval of the manuscript. Magalhães-Gonçalves Dias and Cano were responsible for data curation, processing, visualization, and manuscript writing. Souza-Silva and Capella-Zanotta contributed to the review, revision, validation, and final approval of the manuscript.

### Funding

This study was financed in part by the Coordenação de Aperfeiçoamento de Pessoal de Nível Superior (CAPES), Brazil.

### Conflict of Interest

The authors declare that they have no conflicts of interest.

## References

Alcaras, E., Costantino, D., Guastaferro, F., Parente, C., Pepe, M. 2022. Normalized burn ratio plus (NBR+): A new index for Sentinel-2 imagery. *Remote Sensing*, *14*(8), 1727. https://doi.org/10.3390/rs14071727

Alkan, H., Akıncı, H., Zeybek, M. 2024. Comparison of diverse machine learning algorithms for forest fire susceptibility mapping in Antalya, Türkiye. *Advances in Space Research*. https://doi.org/10.1016/j.asr.2024.04.018

European Space Agency. 2025. *Copernicus Sentinel-2 mission overview*. European Space Agency.

Ballut-Dajud, G.A., Sandoval, C., Lambert, G., Muñiz, L., Méndez, M., Torres, E. 2022. Factors affecting wetland loss: A review. *Land*, *11*(3), 434. https://doi.org/10.3390/land11030434

Basu, S., Basu, K., Ghosh, S., Ganguly, S., Mukhopadhyay, S. 2015. DeepSat: A learning framework for satellite imagery. In Proceedings of the 23rd *SIGSPATIAL International Conference on Advances in Geographic Information Systems* (pp. 1–10). https://doi.org/10.1145/2820783.2820812

Braga, D., Aragão, L.E.O.C., Leão, H., Osborn, F., Wagner, F.H., Cabral, B.F., Dutra, D.J., Izidoro, B., Anderson, L.O., Chaves, J.H., Pantoja, N., Saatchi, S., Dalagnol, R. 2025. Monitoring sustainable logging in an Amazon forest under management using deep learning and Planet NICFI imagery. *International Journal of Remote Sensing*. https://doi.org/10.1080/01431161.2025.2603696

Cho, A., Park, E., Kim, J., Kim, J., Li, C., Song, J. 2023. Burned area mapping using unitemporal PlanetScope imagery with a deep learning-based approach. *IEEE Journal of Selected Topics in Applied Earth Observations and Remote Sensing*, *16*, 242–253. https://doi.org/10.1109/JSTARS.2022.3225070

Chollet, F. 2017. *Deep learning with Python*. Manning.

Dadkhah, H., Rana, D., Ghaderpour, E., Mazzanti, P. 2025. Analyzing wildfire patterns and climate interactions in Campania, Italy: A multi-sensor remote sensing study. *Ecological Informatics, 90*, 103249. https://doi.org/10.1016/j.ecoinf.2025.103249

Dalagnol, R., Wagner, F.H., Chaves, J.H., Pantoja, N.V., Anderson, L.O., Aragão, L.E.O.C., Saatchi, S.S., Souza, C.M. 2023. Mapping tropical forest degradation with deep learning and Planet NICFI data. *Remote Sensing of Environment*, *298*, 113798. https://doi.org/10.1016/j.rse.2023.113798

Dong, H., Wu, H., Sun, P., Ding, Y. 2022. Wildfire prediction model based on spatial and temporal characteristics: A case study of a wildfire in Portugal's Montesinho Natural Park. *Sustainability*, *14*, 10107. https://doi.org/10.3390/su141610107

Dosovitskiy, A., Fischer, P., Ilg, E., Hausser, P., Hazirbas, C., Golkov, V., van der Smagt, P., Cremers, D., Brox, T. 2015. FlowNet: Learning optical flow with convolutional networks. In *Proceedings of the IEEE International Conference on Computer Vision* (pp. 2758–2766). https://doi.org/10.1109/ICCV.2015. 316

Dutra, D.J., Silva, C.V.J., Anderson, L.O., Fonseca, M.G., Silva Junior, C.H.L., Aragão, L.E.O.C. 2022. Fire dynamics in an emerging deforestation frontier in Southwestern Amazonia, Brazil. *Fire*, *6*(1), 2. https://doi.org/10.3390/fire6010002

EMBRAPA. 2018. Pantanal: características gerais. https://www.embrapa.br/pantanal

Erhan, D., Bengio, Y., Courville, A., Manzagol, P.-A., Vincent, P., Bengio, S. 2010. Why does unsupervised pre-training help deep learning? In *Proceedings of the Thirteenth International Conference on Artificial Intelligence and Statistics* (AISTATS) (pp. 201–208). https://doi.org/10.48550/arXiv.1001.0495

Garcia, G., Laparra, V., Lopez, D., Gómez, L. 2020. Cross-sensor adversarial domain adaptation of Landsat-8 and Proba-V images for cloud detection. *IEEE Journal of Selected Topics in Applied Earth Observations and Remote Sensing, 14*, 747–761. https://doi.org/10.1109/JSTARS.2020.3031741.

Gitelson, A.A., Dall'Olmo, G., Moses, W., Rundquist, D.C., Barrow, T., Fisher, T.R., Gurlin, D., Holz, J. 2008. A simple semi-analytical model for remote estimation of chlorophyll-a in turbid waters: Validation. *Remote Sensing of Environment*, *112*(9), 3582–3593. https://doi.org/10.1016/j.rse.2008.04.015

Ghali, R., Akhloufi, M.A. 2023. Deep learning approaches for wildland fires using satellite remote sensing data: Detection, mapping, and prediction. *Fire*, *6*, 192. https://doi.org/10.3390/fire6050192

Goodfellow, I., Bengio, Y., Courville, A. 2016. *Deep learning*. MIT Press.

Gorelick, N., Hancher, M., Dixon, M., Ilyushchenko, S., Thau, D., Moore, R. 2017. Google Earth Engine: Planetary-scale geospatial analysis for everyone. *Remote Sensing of Environment*, *202*, 18–27. https://doi.org/10.1016/j.rse.2017.06.031

Guo, Y., Liu, Y., Oerlemans, A., Lao, S., Wu, S., Lew, M.S. 2016. Deep learning for visual understanding. *Neurocomputing*, *187*, 27–48. https://doi.org/10.1016/j.neucom.2015.09.116

Helber, P., Bischke, B., Dengel, A., Borth, D. 2019. EuroSAT: A novel dataset and deep learning benchmark for land use and land cover classification. *IEEE Journal of Selected Topics in Applied Earth Observations and Remote Sensing, 12*(7), 2217–2226. https://doi.org/10.1109/JSTARS.2019.2918242

Hu, X., Li, S., Xu, J., Zhang, Y., Huang, W. 2021. Uni-temporal multispectral imagery for burned area mapping with deep learning. *Remote Sensing, 13*, 1509. https://doi.org/10.3390/rs13081509

Hinton, G., Srivastava, N., Swersky, K. 2012. *Neural networks for machine learning – Lecture 6a: Overview of mini-batch gradient descent*. University of Toronto.

Huang, J., Rathod, V., Sun, C., Zhu, M., Korattikara, A., Fathi, A., Murphy, K. 2017. Accuracy trade-offs for modern convolutional object detectors. In *Proceedings of the IEEE Conference on Computer Vision and Pattern Recognition* (pp. 7310–7311). https://doi.org/10.1109/CVPR.2017.351

Instituto Brasileiro de Geografia e Estatística (IBGE). 2022. Brasil em síntese: território. IBGE, 2022. Accesible at: https://brasilemsintese.ibge.gov.br/territorio.html.

Kingma, D.P., Ba, J. 2015. Adam: A method for stochastic optimization. In *International Conference on Learning Representations (ICLR)*.

Klemas, V. 2011. Remote sensing of wetlands: case studies comparing practical techniques. *Journal of Coastal Research*, *27*(3), 418-427. https://doi.org/10.2112/JCOASTRES-D-10-00174.1

Krizhevsky, A., Sutskever, I., Hinton, G.E. 2012. ImageNet classification with deep convolutional neural networks. *Advances in Neural Information Processing Systems, 25*, 1097–1105.

Li, W., Sun, K., Wei, J. 2025. Adapting cross-sensor high-resolution remote sensing imagery for land use classification. *Remote Sensing, 17*(5), 927. https://doi.org/10.3390/rs17050927

Lee, S.H., Lee, M.H., Kang, T.H., Cho, H.R., Yun, H.S., Lee, S.J. 2025. Comparative analysis of dNBR, dNDVI, SVM kernels, and ISODATA for wildfire-burned area mapping using Sentinel-2 imagery. *Remote Sensing*. https://doi.org/10.3390/rs17132196

Libonati, R., DaCamara, C.C., Peres, L.F., Sander de Carvalho, L.A., Garcia, L.C. 2020. Rescue Brazil's burning Pantanal wetlands. *Nature, 588*(7837), 217–219. https://doi.org/10.1038/d41586-020-03464-1

Lundberg, S.M., Lee, S. 2017. A unified approach to interpreting model prediction. In *Proceedings of the 31st Conference on Neural Information Processing Systems (NeurIPS 2017)*.

Priya, R.S., Vani, K. 2019. Deep learning-based forest fire classification and detection in satellite images. In *2019 11th International Conference on Advanced Computing (ICoAC)* (pp. 61–65). https://doi.org/10.1109/ICoAC48765.2019.246817

Mataveli, G.A.V., Pereira de Oliveira, G., Seixas, H.T., Cardozo, F.D.S., Shimabukuro, Y.E., Brunsell, N.A. 2021. Pantanal widespread fire: Short- and long-term implications for biodiversity and conservation. *Biodiversity and Conservation, 30*(11), 3299–3303. https://doi.org/10.1007/s10531-021-02243-2

MapBiomas Project. 2024. *MapBiomas Collection 8: Annual land use and land cover maps of Brazil (1985–2022)*. https://doi.org/10.58053/MapBiomas/IBQPF6

Md Jelas, I., Abu Bakar, M.A., Mahmud, M.R., Yusof, K.W., Sulaiman, N. 2024. Deforestation detection using deep learning-based semantic segmentation techniques: a systematic review. *Frontiers in Forests and Global Change*, *7*, 1300060. https://doi.org/10.3389/ffgc.2024.1300060

Instituto Nacional de Pesquisas Espaciais (INPE). 2024. *Queimadas program in Brazil*. https://terrabrasilis.dpi.inpe.br/queimadas/portal/

Srivastava, N., Hinton, G., Krizhevsky, A., Sutskever, I., Salakhutdinov, R. 2014. Dropout: A simple way to prevent neural networks from overfitting. *Journal of Machine Learning Research, 15*, 1929–1958.

Mojica, J.P., Bernini, H., de Faria, D.G., Hauck Antunes, E., Siqueira, L., Souza Silva, C., Rodovalho, F. 2024. Spatialization of fire occurrences in Brazil within the context of the fire events detected by the fire panel. *RAEGA–O Espaço Geográfico em Análise, 60*, 131–158. https://doi.org/10.5380/raega.v60i0.95566

Pazare, H., Raut, P., Dhanorkar, M., Dhage, S. 2022. Forest fire prediction using deep learning. *Forest, 2*(1).

Pérez, D., Risco Ramos, R., Casaverde, L. 2021. Transfer learning for binary classification of thermal images. *Ingenius. Revista de Ciencia y Tecnología, 26*, 71–86.

Pereira, A.D.M.M., Oliveira, M.D.R., Bao, F., Souza, E.B., Pott, A., Escobar, A.C.D.S., Damasceno, G.A. 2024. Changes, trends, and gaps in research dynamics after the megafires in the Pantanal. *Environment, Development and Sustainability*, 1–15.

Sacramento, I.F., Michel, R.F.M., Siqueira, R.G. 2020. Bitemporal analysis of burned areas in the Atlantic Forest. *Sociedade & Natureza*, 32, 540 – 552. https://doi.org/10.14393/SN-v32-2020-53339

Santiago Júnior, V.A. 2024. Empirical evidence regarding few-shot learning for scene classification in remote sensing images. *Applied Sciences, 14*(23), 10776. https://doi.org/10.3390/app142310776

Saha, S., Zhao, S., Shahzad, M., Zhu, X.X. 2022. Mitigating distribution shift for multi-sensor classification. In *IGARSS 2022 – IEEE International Geoscience and Remote Sensing Symposium* (pp. 1201–1204). IEEE. https://doi.org/10.1109/IGARSS46834.2022.9883596

Sausen, T.M. 2007. *Sensoriamento remoto e suas aplicações para recursos naturais*. INPE.

Silva, I.T., Pessi, D.D., da Silva, N.M., Mioto, C.L., Guaraldo, E., Paranhos Filho, A.C. 2021. Técnicas de processamento de imagens para treinamento de fotointerpretes na avaliação visual de áreas úmidas e de manchas e cicatrizes de queimadas ou incêndios. *Revista de Geociências do Nordeste*, 57–67. https://doi.org/10.21680/2447-3359.2021v7n2ID23310

Simonyan, K., Zisserman, A. 2015. *Very deep convolutional networks for large-scale image recognition*. arXiv. https://arxiv.org/abs/1409.1556

Simioni, J.P.D., Guasselli, L.A., Belloli, T.F., Ramos, R.A. 2022. Assessment of fire resilience in subtropical wetlands using high spatial resolution images. *Environmental Monitoring and Assessment, 194*(6), 417. https://doi.org/10.1007/s10661-022-09985-8

Shimabukuro, Y.E., Smith, J.A. 1991. The least-squares mixing models to generate fraction images derived from remote sensing multispectral data. *IEEE Transactions on Geoscience and Remote Sensing, 29*(1), 16–20. https://doi.org/10.1109/36.97458

 EISSN 1988-8740

Tomas, W.M., Berlinck, C.N., Chiaravalloti, R.M., Faggioni, G.P., Strüssmann, C., Libonati, R., Abrahão, C., Alvarenga, G.V., Morato, R.G. 2021. Distance sampling surveys reveal 17 million vertebrates directly killed by the 2020's wildfires in the Pantanal, Brazil. *Scientific Reports*, *11*, 23547. https://doi.org/10.1038/s41598-021-02844-5.

Singh, S.S., Jeganathan, C. 2024. Using ensemble machine learning algorithm to predict forest fire occurrence probability in Madhya Pradesh and Chhattisgarh, India. *Advances in Space Research, 73*(6), 2969–2987. https://doi.org/10.1016/j.asr.2024.01.014

Unnikrishnan, A., Reddy, C.S. 2020. Characterizing distribution of forest fires in Myanmar using earth observations and spatial statistics tool. *Journal of the Indian Society of Remote Sensing, 48*(2), 227–234. https://doi.org/10.1007/s12524-019-01023-1

Viganó, H.H. da G., Souza, C.C. de, Cristaldo, M.F., Jesus, L. de. 2017. Redes neurais artificiais na previsão de queimadas e incêndios no Pantanal. *Revista Brasileira de Geografia Física, 10*(5), 1355–1367. https://doi.org/10.26848/rbgf.v.10.p1355-1367

Wahab, M.A.A., Abdullah, A.F., Shafri, H.Z.M., Hamedianfar, A., Yusoff, A.R. 2021. Mapping deforestation in permanent forest reserve of Peninsular Malaysia with multi-temporal SAR imagery and U-Net based semantic segmentation. *Remote Sensing*, *13*, 2430. https://doi.org/10.3390/rs13132430

Yandouzi, M., Grari, M., Idrissi, I., Boukabous, M., Moussaoui, O., Azizi, M. 2022. Forest fires detection using deep transfer learning. *International Journal of Advanced Computer Science and Applications, 13*(8), 268–275. https://doi.org/10.14569/IJACSA.2022.0130832

Yin, X., Chen, W., Wu, X., Yue, H. 2017. Fine-tuning and visualization of convolutional neural networks. In *2017 12th IEEE conference on industrial electronics and applications (ICIEA)*, 1310-1315. https://doi.org/10.1109/ICIEA.2017.8283041

Zhou, W., Newsam, S., Li, C., Shao, Z. 2018. A benchmark dataset for performance evaluation of remote sensing image retrieval. *ISPRS Journal of Photogrammetry and Remote Sensing, 145*, 197-209. https://doi.org/10.1016/j.isprsjprs.2018.01.004